

# The electrochemical properties of MgNi- $x$ wt% TiNi<sub>0.56</sub>Co<sub>0.44</sub> ( $x = 0, 10, 30, 50$ ) composite alloys

Hongxia Huang · Kelong Huang · Dongyang Chen ·  
Suqin Liu · Shuxin Zhuang

Received: 26 June 2009 / Accepted: 21 November 2009 / Published online: 5 December 2009  
© Springer Science+Business Media, LLC 2009

**Abstract** The effect of ball milling time and different content of the TiNi<sub>0.56</sub>Co<sub>0.44</sub> alloy on the structure and electrochemical properties of MgNi- $x$  wt% TiNi<sub>0.56</sub>Co<sub>0.44</sub> ( $x = 0, 10, 30, 50$ ) alloys were studied systematically. The results indicated that the cycle durability of the alloy was improved with addition of the TiNi<sub>0.56</sub>Co<sub>0.44</sub> alloy. By cyclic voltammetry (CV) and electrochemical impedance spectroscopy (EIS) analysis, it was shown that the introduction of the TiNi<sub>0.56</sub>Co<sub>0.44</sub> alloy could significantly improve the catalytic activity of the electrode, decrease the charge-transfer reaction resistance and the diffusion impedance of H atoms. Potentiodynamic polarization curves revealed that anti-corrosion performance of the composite electrodes was enhanced, which was responsible for the ameliorative cycle stability of composite alloys. A high discharge capacity and good cycle stability had been observed for the  $x = 10$  (10 h) composite electrode with a maximum discharge capacity of 397 mAh/g and capacity retaining rate ( $S_{50}$ ) of 62%.

## Introduction

Mg-based alloys are considered to be one of the most promising candidates for the Ni-MH batteries negative

electrode material owing to their unique potentials such as high hydrogen storage capacity, light weight, low production cost, interchangeability with the Cd-Ni batteries, and abundance in natural resources [1]. However, practical application of Mg-based alloys is inhibited due to poor hydriding/dehydriding kinetics at room temperature and unfavorable charge/discharge cycle stability [2]. The pursuit of increasing the cycle capacity of this kind of alloys has been one of the main challenges faced by researchers in this field. Many efforts have been made to improve the cycle stability and the kinetic characteristics of alloy electrode, including element substitution [3, 4], surface modifications [5–7], powder sieving [8], and formation of alloy composite [9–12]. Composite alloys have proved to be very effective for improving the general characteristics of alloy electrodes. Santos et al. [13] reported that the mechanical coating of a Mg–50 at.% Ni alloy with Ni and Ni–5 at.% Al could improve the cycle life performance of the Mg–Ni metastable alloys. He et al. [1] found that the cycle stability of MgNi was improved by addition of CoB and TiB. The La<sub>0.7</sub>Mg<sub>0.25</sub>Zr<sub>0.05</sub>Ni<sub>2.975</sub>Co<sub>0.525</sub> alloy could significantly improve the discharge capacity of Ti<sub>0.9</sub>Zr<sub>0.2</sub>Mn<sub>1.5</sub>Cr<sub>0.3</sub>V<sub>0.3</sub> alloy [14] and the discharge capacity of Ti–V-based BCC phase alloy was increased by the introduction of LaNi<sub>5</sub> alloy [15]. Si [16] observed that the activation behavior of Mg<sub>2</sub>Ni alloy was improved significantly by the addition of LaNi<sub>5</sub> alloy. Although lots of investigations on the Mg-based alloy were carried out and some important progresses have been obtained, it is a long distance to take Mg-based alloy from laboratory to market. The key problem is still how to improve the cycle stability of the alloy.

As the Ti-based AB-type Laves phase hydrogen storage material, TiNi has many advantages including high charge/discharge efficiency, excellent anti-corrosion performance, and small lag phenomena. In view of the advantages of

H. Huang · K. Huang (✉) · D. Chen · S. Liu · S. Zhuang  
College of Chemistry and Chemical Engineering, Central South  
University, Changsha 410083, People's Republic of China  
e-mail: huangkelong@yahoo.com.cn

H. Huang  
e-mail: hhx\_hunan@yahoo.com.cn

H. Huang  
College of Chemistry and Biological Engineering,  
Guilin University of Technology, Guilin 541004,  
People's Republic of China

MgNi alloy and TiNi alloy, it can be expected that a novel composite alloy electrode with high discharge capacity and good cycle stability could be obtained through incorporating MgNi with TiNi-type alloy.

In this work, the composites were prepared by ball milling MgNi with different content of  $\text{TiNi}_{0.56}\text{Co}_{0.44}$  alloy, which resulted in appreciable increase of the cycle stability of the composite electrodes. The phase structure and electrochemical properties of  $\text{MgNi}-x \text{ wt\% TiNi}_{0.56}\text{Co}_{0.44}$  ( $x = 0, 10, 30, 50$ ) composite alloys were studied.

## Experimental

### Preparation of the alloys

MgNi alloy was prepared by ball milling (MA) of pure magnesium powder and nickel powder (200 mesh) in a stainless steel vessel under argon atmosphere using a planetary ball mill (ND7-2L, Nanjing), the mass ratio of stainless milling balls to powders was 20:1, and the purity of all the metallic powders was higher than 99.0%. The milling speed was 250 rpm and the duration was 90 h.  $\text{TiNi}_{0.56}\text{Co}_{0.44}$  alloy was prepared by ball milling the constituent elements (300 mesh) in a similar method except for the milling time was 100 h. The composites were prepared by ball milling the homogenous mixture of MgNi and  $x \text{ wt\% TiNi}_{0.56}\text{Co}_{0.44}$  ( $x = 10, 30, 50$ ) for 10, 15, and 30 h.

### Apparatus and electrochemical measurements

The structures and surface morphologies of the alloys were measured by powder X-ray diffraction using Japan D/max 2550 VB + 18 kV diffractometer ( $\text{CuK}_\alpha$  radiation,  $\lambda = 1.54178 \text{ \AA}$ ) and scanning electron microscopy (SEM, JSM-6360 LV).

The test electrodes were fabricated according to the following procedure: Cold pressing a mixture of 0.10 g alloy powder with 0.20 g carbonyl nickel powder into a pellet of 10 mm in diameter under a pressure of 10 MPa and then pressed at 20 MPa between two pieces of foam nickel. Electrochemical measurements were conducted by using a land 5.3 B Battery Test instrument (CT2001C) in a two compartment cell, consisting of a working electrode (as-prepared electrode), a sintered  $\text{NiOOH}/\text{Ni}(\text{OH})_2$  counter electrode (purchased from Hunan Kaifeng New Energy Co., Ltd.). The electrolyte solution was 6 mol/L KOH aqueous solution. In each charge/discharge cycle test, the electrode was charged for 6 h at a current density of 100 mA/g and discharged at 50 mA/g to the cut-off voltage of 1.0 V. The testing time between charge and discharge was 5 min.

During EIS, CV, and potentiodynamic polarization tests, HgO/Hg electrode was used as reference electrode. CS 300

electrochemical workstation was used for potentiodynamic polarization (scanning rate: 0.1 mV/s, potential range:  $-1.0 \sim -0.4 \text{ V vs. HgO/Hg}$ ) and cyclic voltammogram (scanning rate: 0.1 mV/s, potential range:  $-1.0 \sim -0.4 \text{ V vs. HgO/Hg}$ ). IM 6 electrochemical workstation apparatus was used for EIS measurement (amplitude: 5 mV, frequency range:  $10^3 \text{ Hz} \sim 10^{-3} \text{ Hz}$ ). In order to reduce the ohmic drop between the working electrode and the reference electrode, a Luggin capillary was located close to the working electrode.

## Results and discussion

### Phase structure

Figure 1 shows the X-ray diffraction patterns of the MgNi alloy and the  $\text{MgNi}-x \text{ wt\% TiNi}_{0.56}\text{Co}_{0.44}$  ( $x = 10, 30, 50$ ) composites MA for 10 h. A broad peak appears in the region of  $40\text{--}50^\circ$  for MgNi alloy, suggesting that the alloy has formed a main amorphous structure. After ball milling with different content of  $\text{TiNi}_{0.56}\text{Co}_{0.44}$  for 10 h, it is found that the intensity of the band increases and its position shifts towards higher angle, which implies that the atomic arrangement in composite sample becomes more ordered and the  $\text{TiNi}_{0.56}\text{Co}_{0.44}$  alloy has dissolved in the main MgNi amorphous phase. There is no obvious distinction in the phase structures between the 15, 30 h samples and the 10 h samples, so the XRD patterns of the composite alloys milled for 15 and 30 h are not given.

### Surface morphology

Figure 2 shows the SEM micrographs of the MgNi alloy and the  $x = 10$  (10 h) composite alloy. It is obvious that

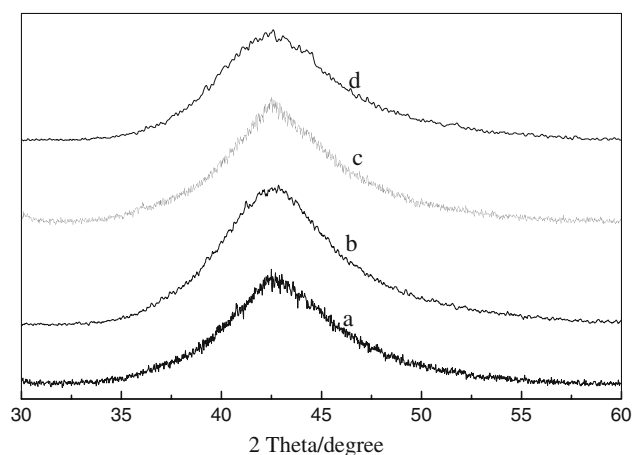


**Fig. 1** The XRD patterns of the MgNi alloy and the  $\text{MgNi}-x \text{ wt\% TiNi}_{0.56}\text{Co}_{0.44}$  ( $x = 10, 30, 50$ ) composite alloys MA for 10 h. (a) MgNi; (b)  $x = 10$  (10 h); (c)  $x = 30$  (10 h); and (d)  $x = 50$  (10 h)

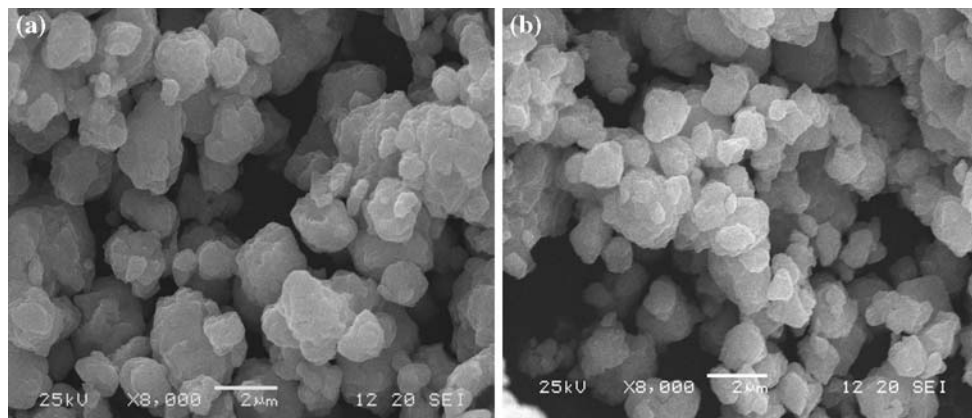


**Fig. 2** The SEM micrographs of **a** MgNi alloy and **b**  $x = 10$  (10 h) alloy

after ball milling MgNi and  $\text{TiNi}_{0.56}\text{Co}_{0.44}$  mixture powders, the particle of composite alloy becomes smaller and the interspaces are more uniform than that of the pure MgNi alloy, from which the electrode performance will benefit.

#### Discharge capacity and cycle behavior

The cycle number dependence of the discharge capacity of the  $\text{MgNi}-x$  wt%  $\text{TiNi}_{0.56}\text{Co}_{0.44}$  ( $x = 0, 10, 30, 50$ ) alloy electrodes was plotted in Fig. 3. An outstanding characteristic from a commercial point of view is that the alloy electrodes can be activated at the first cycle, so an activation process is unnecessary as it is the case for other alloy electrodes [17, 18]. The decisive factors of the activation capability of the alloy are phase structure, surface state, grain size, composition homogeneity, and interstitial dimensions of the alloy [19]. The alloy electrodes have good activation performance, which is attributed to their mainly amorphous structures. Amorphous alloy powder constitutes an overlapping area of alloys and nanophase materials and excellent activation performance is derived from the combination of their disordered structure and nanoscale size [20, 21]. Liu and Suda [22] confirmed that the amorphous alloy can provide more supplementary paths with lower activation energy for hydrogen diffusion and more relaxed interstitial sites for hydrogen occupation. As a result, amorphous alloy has a larger H-capacity and more rapid kinetics compared with the corresponding crystalline alloy [23].

The capacity retaining rate ( $S_n$ ) used to characterize the cycle stability can be calculated by the following expression:

$$S_n(\%) = C_n/C_{\max} \times 100 \quad (1)$$

where the  $C_n$  is the discharge capacity at cycle number  $n$  and the  $C_{\max}$  is the maximum discharge capacity. The

information on the cycle stability of the  $\text{MgNi}-x$  wt%  $\text{TiNi}_{0.56}\text{Co}_{0.44}$  ( $x = 0, 10, 30, 50$ ) alloy electrodes is presented in Table 1. The MgNi alloy electrode has the highest initial discharge capacity (444 mAh/g) and the worst cycle stability. After introduction of  $\text{TiNi}_{0.56}\text{Co}_{0.44}$  alloy, the cycle stability of the alloy was improved evidently at the cost of the maximum discharge capacity. Among the composite electrodes, the  $x = 10$  (10 h) alloy shows the highest discharge capacity (397 mAh/g) and the best cycle stability. After 50 cycles, the capacity is 248 mAh/g and the capacity retaining rate is 62%. The improvement of cycle stability is ascribed to the introduction of  $\text{TiNi}_{0.44}\text{Co}_{0.56}$ . Generally speaking, titanium can form a dense passive oxide in alkaline solution, which inhibits the oxidation of magnesium on the alloy surface [24] and favors the cycle stability of alloy electrodes.

As seen from Table 1, the cycle performance of the electrode alloys with different composite time performs differently. The deterioration of the discharge capacity can be explained by the oxidation-pulverization principles. (1) In KOH solution, the Mg on the surface of the particles takes place serious oxidation and corrosion to loose gel-type  $\text{Mg}(\text{OH})_2$ , which cannot prevent the electrolyte from corroding the alloy further, moreover, it baffles the diffusion of hydrogen atoms in the process of hydrogen absorption and desorption. (2) The pulverization of the alloys due to the expansion and contraction of cell volume leads to the accentuation of corrosion and oxidation. The SEM micrographs of the MgNi alloy electrode before and after 50 charge/discharge cycles are shown in Fig. 4. It is noteworthy that the particle surface morphology for the alloy changes from smooth to rough and a white oxidation and corrosion layer can be seen on the surface of the alloy after the electrochemical cycle. This indicates that pulverization and corrosion of the alloy electrode are extremely important factors that lead to the capacity deterioration of the electrode.

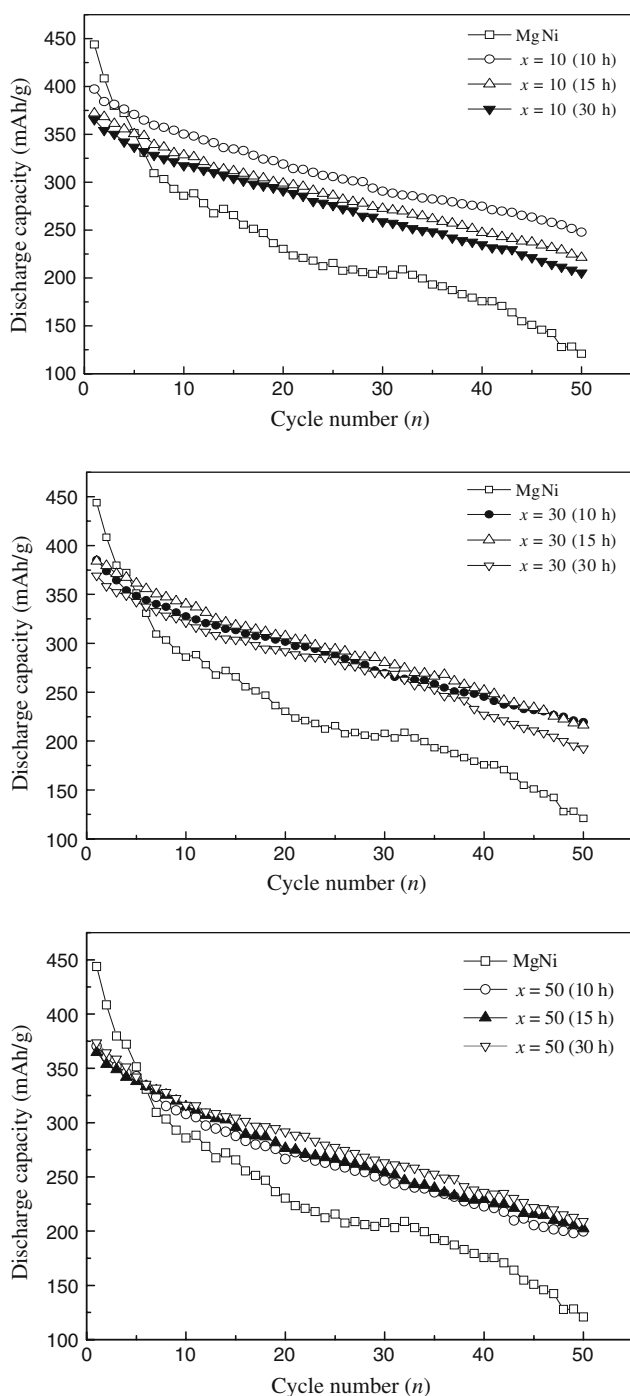


**Fig. 3** The discharge capacity of the MgNi and the MgNi- $x$  wt% TiNi<sub>0.44</sub>Co<sub>0.56</sub> ( $x = 0, 10, 30, 50$ ) composite alloy electrodes

For a fixed TiNi<sub>0.56</sub>Co<sub>0.44</sub> content  $x$  ( $x = 10, 30$ ), the extending of milling time deteriorates the maximum discharge capacity and the capacity retaining rate of composite alloys, for which the following two reasons are primarily responsible. One is that with extending of ball milling time from 10 to 30 h, some imperceptible crystal

**Table 1** The cycle stability of MgNi- $x$  wt% TiNi<sub>0.56</sub>Co<sub>0.44</sub> ( $x = 0, 10, 30, 50$ ) alloy electrodes

Samples	$C_{\max}$	$C_{30\text{th}}$	$S_{30}$ (%)	$C_{50\text{th}}$	$S_{50}$ (%)
MgNi	444	208	47	121	27
$x = 10$ (10 h)	397	291	73	248	62
$x = 10$ (15 h)	372	272	73	221	59
$x = 10$ (30 h)	365	259	71	205	56
$x = 30$ (10 h)	385	270	70	219	57
$x = 30$ (15 h)	384	280	73	216	56
$x = 30$ (30 h)	369	269	73	192	52
$x = 50$ (10 h)	370	247	67	200	54
$x = 50$ (15 h)	365	254	70	202	55
$x = 50$ (30 h)	374	263	70	209	56

structure appears in the alloy, which can enhance the anti-corrosion behavior. The other is that the size of alloy particles is diminished, increasing the ratio of expansion/contraction of the alloy electrode in the process of hydrogen absorption/desorption, which means decreasing the anti-pulverization ability of alloy electrode. Some composite alloy particles are finally pulverized and deposited in the electrolyte, consequently, leads to the loss of the discharge capacity. It is the above contrary effects that result in an optimum milling time for the cycle stability of alloy electrode. In this investigation, the latter reason should be a predominant factor for the deterioration of the cycle durability of the composite electrodes with prolonging ball milling. The  $x = 50$  alloy needs more milling time to reach the maximum discharge capacity. According to the reference [1], more milling time can make TiNi<sub>0.44</sub>Co<sub>0.56</sub> alloy dissolved in the host phase and creating more crystal lacunas, which are in favor of absorbing and desorbing H atoms. It is believed that TiNi<sub>0.44</sub>Co<sub>0.56</sub> has good electrocatalytic activity for the hydrogen electrode reaction in alkaline solution. After ball milling, the TiNi<sub>0.44</sub>Co<sub>0.56</sub> particles can be dispersed on the MgNi alloy surface, therefore, acting as the catalytic active sites for the hydrogen electrode reaction. Increased defect density from ball milling may improve the diffusion of hydrogen in the alloy particles, which is also believed to be beneficial for improving hydriding/dehydriding reactions.

According to the charge/discharge results, ball milling MgNi with 10% TiNi<sub>0.44</sub>Co<sub>0.56</sub> for 10 h is the best treatment to obtain an alloy with high discharge capacity and good cycle performance.

#### Cyclic voltammogram (CV)

To further demonstrate the phenomena described above in detail, the CV curves of the MgNi alloy and the  $x = 10$  alloys are depicted in Fig. 5.

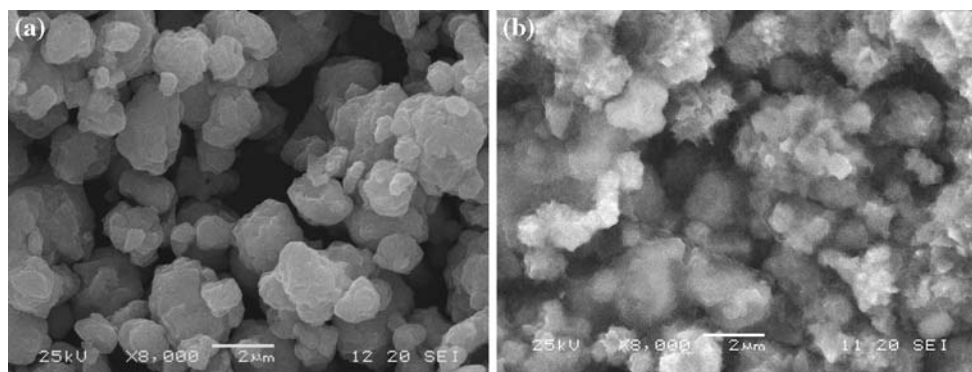


**Fig. 4** SEM micrographs of the MgNi alloy electrode before and after 50 cycles. **a** Before cycle and **b** after 50 cycles

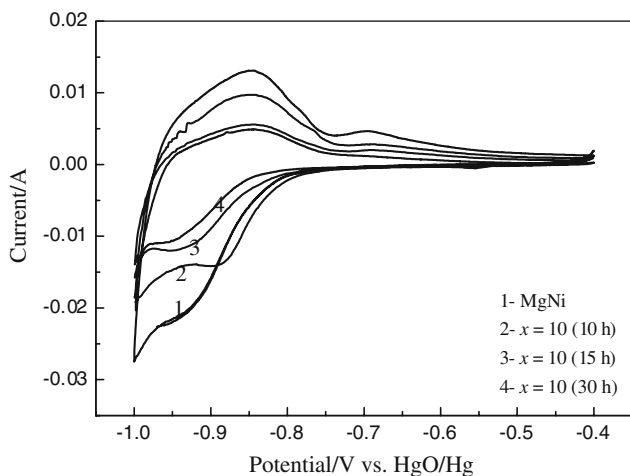


**Fig. 5** The CV curves of the MgNi and the  $x = 10$  composite alloy electrodes

The anodic peak at around  $-0.85$  V vs. HgO/Hg is attributed to the oxidation of hydrogen absorbed in the alloy according to the following equation [25]:



The value of  $I_p$  can be used to evaluate the electrode catalytic activity of hydride electrode [26], and the larger of the  $I_p$  indicates the better of electro-catalytic activity. It can be derived from Fig. 5 that the kinetics of the electrodes is in order of  $MgNi > x = 10$  (10 h)  $> x = 10$  (15 h)  $> x = 10$  (30 h). The peak area is ascribed to the capacity of hydrogen desorption, the larger peak area indicates the higher discharge capacity [27], the variation of peak area is consistent with that of the maximum discharge capacity shown in Table 1. The cathodic peak at around  $-0.95$  V vs. HgO/Hg is attributed to the hydriding reaction according to above equation at the opposite side. It is observed that the difference between the anodic peak potential and the cathodic peak potential enlarged with increasing the composite time, which means the reversibility of the electrode becomes worse.

All those results mentioned above indicate that the kinetics of the electrochemical hydrogen reaction in the composite electrode are deteriorated with extending milling time, which may be due to the following reason. With the ball milling carrying on, the particles of composite alloy become smaller, which increase of the electrode oxidation due to a larger surface area in contact with the electrolyte. In addition, the oxide layer baffles the diffusion of hydrogen atoms and would certainly weaken its dynamical property in the process of hydrogen absorption and desorption.

Electrochemical impedance spectra (EIS) test

Figure 6 presents the EIS Nyquist diagrams for the MgNi and  $x = 10$  alloy electrodes. Each spectra consists of a semicircle followed by a sloped straight line. The semicircle at high-frequency was ascribed to the charge-transfer reaction resistance and the line at low frequency to the Warburg impedance the of H atoms diffusion from surface of the alloy to the inner phase [28]. The semicircles of the

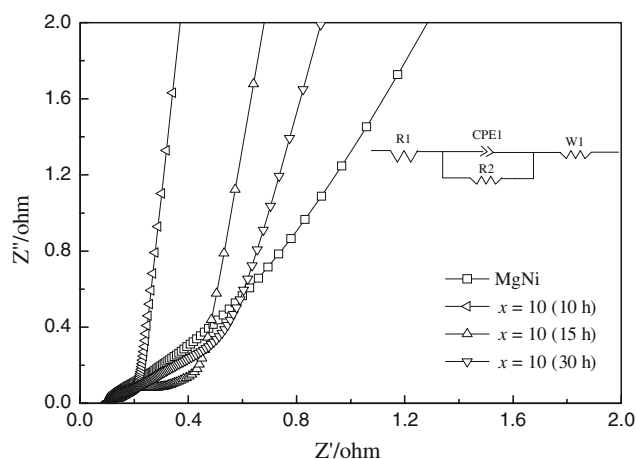
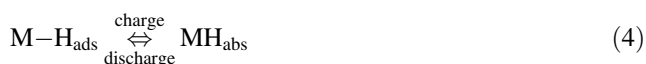
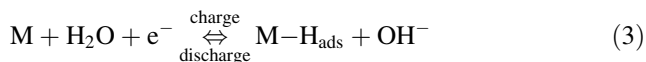


**Fig. 6** The electrochemical impedance spectroscopy for the MgNi and the  $x = 10$  composite alloy electrodes

$x = 10$  composite alloys are smaller than that of MgNi alloy, implying the values of the electrochemical resistance ( $R_2$ ) are smaller than that of MgNi alloy. As for the  $x = 10$  alloys, the semicircle for the 10 h composite is smallest, followed by 15 and 30 h composites. A proposed equivalent circuit for the frequency response of the tested alloy electrodes is inserted in Fig. 6. In which,  $R_1$  is the electrolyte resistance,  $CPE_1$  is the constant-phase element,  $R_2$  is the charge-transfer reaction resistance on the alloy electrode surface and  $W_1$  is the Warburg impedance of hydrogen in the bulk alloy. On the basis of the equivalent circuit and by means of the nonlinear least fitting program Z-View, the values of charge-transfer reaction resistance ( $R_2$ ) and the Warburg resistance ( $W_1$ ) were summarized in Table 2.

It is well known that the electrochemical reactions taking place at the metal hydride electrode in KOH electrolyte during charging/discharging can be expressed as follows [29]:



In which, M is the hydrogen storage alloy,  $M-H_{\text{ads}}$  denotes the adsorbed hydrogen on the surface of the metal hydride and  $MH_{\text{abs}}$  refers to the absorbed hydrogen in the bulk of the metal hydride. It can be derived from Eqs. (3) and (4) that the discharge kinetics of the alloy electrode is controlled not only by the charge-transfer reaction occurring at the interface of alloy/electrolyte, but also by the hydrogen diffusion process from the interior of the bulk to the surface of the alloy particles [30].

From the above analysis, it can be concluded that the electrochemical hydrogen reaction kinetics in the composite electrode is improved, which is ascribed to the existence of  $TiNi_{0.56}Co_{0.44}$  alloy on the surface of the alloy. After  $TiNi_{0.56}Co_{0.44}$  alloy was introduced to MgNi alloy, the content of Ni element increases. According to the previous study [31], Ni element possesses good electrocatalytic activity and good corrosion resistance in an alkaline solution, which results in the improvement of charge-transfer reaction of the metal hydride electrode and the H atoms diffusion from the surface to the bulk of the alloy.

**Table 2** The EIS simulated electrochemical parameters of the MgNi and the  $x = 10$  alloy electrodes

Samples	MgNi	$x = 10$ (10 h)	$x = 10$ (15 h)	$x = 10$ (30 h)
$R_2$ ( $\Omega$ )	3.674	0.185	0.216	0.567
$W_1$ ( $\Omega$ )	1.433	0.410	0.345	0.309

## Potentiodynamic polarization

Many studies about the corrosion behavior of the alloy are performed because the corrosion of the alloy composition is a barrier to its commercial application [32]. To confirm the effect of  $TiNi_{0.56}Co_{0.44}$  on corrosion resistance, potentiodynamic polarization was employed to investigate the corrosive behavior of the alloy electrode. Figure 7 presents the potentiodynamic polarization curves of the MgNi and the  $x = 10$  alloy electrodes. Each polarization curve includes an anode and a cathode polarization process.

The results obtained by Tafel fitting are highlighted in Table 3. It is generally accepted that more positive corrosion potential ( $E_{\text{corr}}$ ) and smaller corrosion current density ( $I_{\text{corr}}$ ) results in the improved corrosion resistance of the electrode. The values of  $E_{\text{corr}}$  is in the order of  $x = 10$  (10 h)  $>$   $x = 10$  (15 h)  $>$   $x = 10$  (30 h)  $>$  MgNi, which is in agreement with the results of cycle stability. The root cause for the deactivation of the battery is the negative electrode rather than the positive electrode. The failure of the battery is characterized by the decay of the discharge capacity and the decrease of the discharge voltage. Literature [18] confirmed that the fundamental reasons for the deterioration of discharge capacity of the alloy electrodes are the pulverization of the alloy particles during consecutive hydrogenation/dehydrogenation and the oxidation/corrosion of alloy components in an alkaline electrolyte. During ball milling,  $TiNi_{0.56}Co_{0.44}$  alloy can be easily

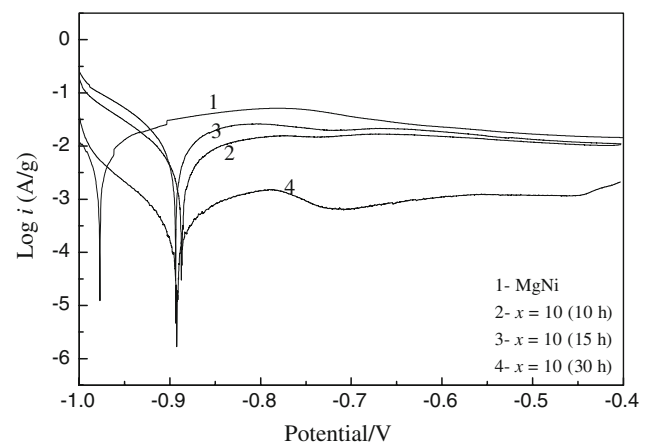


**Fig. 7** The potentiodynamic polarization curves of the MgNi and the  $x = 10$  composite alloy electrodes

**Table 3** The Tafel fitting data of the MgNi and the  $x = 10$  alloy electrodes

Samples	MgNi	$x = 10$ (10 h)	$x = 10$ (15 h)	$x = 10$ (30 h)
$E_{\text{corr}}$ (V)	-0.977	-0.887	-0.892	-0.893
$I_{\text{corr}}$ ( $A/cm^2$ )	0.052	0.016	0.030	0.001

cohered on the surface of MgNi alloy particles, helping to improve the electrochemical catalytic activity significantly, which is responsible for the improvement of cycle stability of the composite alloys. It is proved that an effective approach of strengthening the cycle capability of alloy electrode is enhancing the anti-corrosion and anti-oxidation capabilities of the alloys in an alkaline electrolyte.

## Conclusions

In this work, the MgNi- $x$  wt% TiNi<sub>0.56</sub>Co<sub>0.44</sub> ( $x = 0, 10, 30, 50$ ) alloys were prepared and their electrochemical characteristics were studied. The results showed that the cycle stability of the composite alloys was noticeably improved due to increased corrosion resistance of the TiNi<sub>0.56</sub>Co<sub>0.44</sub> alloy. CV, EIS, and potentiodynamic polarization suggested that the surface electrocatalytic activity of the composite electrodes increased and the hydrogen absorption/desorption kinetics improved due to the introduction of TiNi<sub>0.56</sub>Co<sub>0.44</sub> alloy. Among the investigated alloys, the milled for 10 h with 10 wt% TiNi<sub>0.56</sub>Co<sub>0.44</sub> composite alloy electrode exhibited the best overall electrochemical performance.

**Acknowledgements** This work was financially supported by the National Natural Science Foundation of China (50772133) and the Open Subject of State of Key Laboratory for Powder Metallurgy of Central South University (2008112009).

## References

- He G, Jiao LF, Yuan HT, Zhang YY, Wang YJ (2008) *J Alloys Compd* 450:375
- Liu JW, Jiao LF, Yuan HT (2005) *J Alloys Compd* 403:270
- Zhang YH, Zhao DL, Li BW, Ren HP, Guo SH, Wang XL (2007) *J Mater Sci* 42:8172. doi:10.1007/s10853-007-1689-4
- Yuan HT, Li QD, Song HN, Wang YJ, Liu JW (2003) *J Alloys Compd* 353:322
- Liu FJ, Suda S (1996) *J Alloys Compd* 232:212
- Hatano YJ, Tachikawa T, Mu D, Abe T, Watanabe K, Morozumi S (2002) *J Alloys Compd* 330–332:816
- Huang HX, Huang KL, Liu SQ, Zhuang SX, Chen DY (2009) *J Mater Sci* 44:4460. doi:10.1007/s10853-009-3676-4
- Rongeat C, Grosjean MH, Ruggeri S, Dehmas M, Bourlot S, Marcotte S, Roué L (2006) *J Power Sources* 158:747
- Wang Y, Qiao SZ, Wang X (2008) *Int J Hydrogen Energy* 33:1023
- Chu HL, Qiu SJ, Sun LX, Zhang Y, Xu F, Zhu M, Hu WY (2008) *Int J Hydrogen Energy* 33:755
- Pal K (1997) *J Mater Sci* 32:5177. doi:10.1023/A:1018633358920700
- Gao Y, Zeng MQ, Li BL, Zhu M (2003) *J Mater Sci* 38:2499. doi:10.1023/A:1023921605728
- Santos SF, De Castro JFR, Ishikawa TT, Ticianelli EA (2008) *J Mater Sci* 43:2889. doi:10.1007/s10853-007-1924-z
- Chu HL, Zhang Y, Sun LX, Qiu SJ, Xu F, Yuan HT (2007) *Int J Hydrogen Energy* 32:1898
- Yu XB, Walker GS, Grant DM, Wu Z, Xia BJ, Shen J (2005) *Appl Phys Lett* 87:133121
- Si TZ, Zhang QA (2006) *J Alloys Compd* 414:317
- Zhang YH, Li BW, Ren HP, Wu ZW, Cai Y, Wang XL (2007) *Mater Chem Phys* 105:86
- Miao H, Pan HG, Zhang SC, Chen N, Li R, Gao MX (2007) *Int J Hydrogen Energy* 32:3387
- Zhang YH, Li BW, Zhao DL, Ren HP, Cai Y, Dong XP, Wang XL (2007) *Int J Hydrogen Energy* 32:3420
- Wang MW, Li FY, Zhang RB (2004) *Catal Today* 93–95:603
- He YG, Qiao MH, Hu HR, Pei Y, Li HX, Deng JF (2002) *Mater Lett* 56:952
- Liu FJ, Suda S (1995) *J Alloys Compd* 231:696
- Li L, Wu DC, Liang GY, Sun ZB, Guo YL (2009) *J Alloys Compd* 474:378
- Iwakura C, Shin-ya R, Miyahara K, Nohara S, Inoue H (2001) *Electrochim Acta* 46:2781
- Chen Y (1998) *Catal Today* 44:3
- Guo ZP, Huang ZG, Konstantinov K, Liu HK, Dou SX (2006) *Int J Hydrogen Energy* 31:2032
- Kitmura T, Iwakura C, Tamura H (1982) *Electrochim Acta* 29:1729
- Kuriyama N, Sakai T, Miyamura H, Uehara I, Ishikawa H, Iwasaki T (1993) *J Alloys Compd* 202:183
- Tian QF, Zhang Y, Tan ZC, Sun LX, Xu F, Yuan HF (2006) *Acta Phys Chim Sin* 22(3):301
- Ma S, Gao MX, Li R, Pan HG, Lei YQ (2008) *J Alloys Compd* 457:457
- Wang Y, Wang X, Gao XP, Shen PW (2007) *Int J Hydrogen Energy* 32:4180
- Liu N, Wang JL, Wu YM, Wang LM (2008) *J Mater Sci* 43:2550. doi:10.1007/s10853-008-2447-y